International Journal of Multiphase Flow 34 (2008) 916–923

Contents lists available at ScienceDirect

International Journal of Multiphase Flow

journal homepage: www.elsevier.com/locate/ijmulflow

Heavy particle dispersion from a point source in turbulent pipe flow

Abdallah S. Berrouk [a,*], David E. Stock [b,1], Dominique Laurence [c,2], James J. Riley [d,3]

[a] The University of Manchester, MACE School, P.O. Box 88, Manchester M60 1QD, UK
[b] Washington State University, MME School, Pullman, WA 99164, USA
[c] Electricite de France, R&D, MFEE, 6 Quai Watier 78400, Paris, France
[d] University of Washington, Mech. Eng. Department, Seattle, WA 98116, USA

ARTICLE INFO

Article history:
Received 30 September 2007
Received in revised form 24 April 2008
Available online 10 May 2008

Keywords:
Heavy particle dispersion
LES
Cross-trajectory effects
Drift parameter
Time scales

ABSTRACT

Dispersion of heavy particles from a point source in high-Reynolds pipe flow was studied using large-eddy simulation, LES. A stochastic Langevin type Lagrangian model developed by Berrouk et al. was used to account for heavy particle transport by the sub-grid scale motion. In both the LES and in an experiment by Arnason, the larger particles dispersed more than the small ones. The change in diffusivity with particle size is interpreted in terms of the effect of inertia and cross-trajectory effects and qualitatively compared with the analysis of heavy particle dispersion in isotropic turbulence by Wang and Stock. Particle inertia has a much larger influence on the dispersion than the crossing-trajectories effects.

1. Introduction

The dispersion of heavy particles from a point source in turbulent flows is of practical interest in a wide range of industrial and environmental flows. The distribution of particles after they are injected into combustion chambers or when they are travelling in pipes plays a key role in the efficiency and stability of energy conversion and transport processes. Also, the effectiveness of the atmospheric boundary layer in dispersing particulate pollutants and aerosols that originate from a point source to acceptable concentration levels is of interest to regulatory agencies.

Because dispersion of fluid particles in a turbulent flow is a basic element in turbulence, analysis of the phenomenon has attracted considerable attention in the decades since the pioneering work of Taylor (1921). Taylor established the fundamental theory for turbulent diffusion of fluid elements originating from a point source. Taylor's work has also been the starting point for theoretical studies of heavy particle dispersion over the last 60 years. Analyses by Nir and Pismen (1979) and Reeks (1977) predicted the possibility of solid particles dispersing faster than fluid particles in homogeneous and isotropic turbulence. Crowe et al. (1985) showed that heavy particles with intermediate Stokes numbers can disperse significantly faster than the flow due to the centrifugal effects created by free shear flows. The work of Calabrese and Middleman (1979), Jones (1966) and Arnason and Stock (1983) show that, under certain conditions, large heavy particles can disperse faster than small particles and faster than fluid particles.

Taylor's theory (Taylor, 1921) provides a framework for understanding Arnasons experimental findings by accounting for both gravity and cross-trajectory effects resulting from the presence of a body force. In Taylor's approach, particle dispersion in isotropic and stationary turbulence is linked to the particle rms fluctuating velocity v'_p and the particle Lagrangian time scale T_{Lp}:

$$\epsilon_p = v'^2_p \cdot T_{Lp}. \tag{1}$$

Particle inertia causes heavy particles to respond sluggishly to fluid turbulence (Tchen, 1947), and not follow the high-frequency turbulent fluctuations. As the particle inertia increases, v'_p decreases and T_{Lp} increases. The particle Lagrangian integral time scale increases because the particle, once set in motion by a large turbulent fluctuation, continues moving in that direction longer due to its high inertia. Thus the dispersion coefficient ϵ_p can increase or decrease with increasing inertia, depending on the relative change in v'_p and T_{Lp}.

The motion of heavy particles is affected by body forces resulting from gravity, electric fields (if the particle is charged), and magnetic fields (if the particle is magnetic), which cause the particle to have an average velocity not equal to the average fluid velocity. The effect of this relative velocity on particle dispersion is known

* Corresponding author. Present address: Department of Building and Construction, City University of Hong Kong, Tat Chee Avenue, Kowloon City, Kowloon, Hong Kong. Tel.: +852 3442 5715.
E-mail addresses: berrouks@yahoo.fr, aberrouk@cityu.edu.hk, a.berrouk@postgrad.manchester.ac.uk (A.S. Berrouk), stock@wsu.edu (D.E. Stock), dominique.laurence@edf.fr (D. Laurence), rileyj@u.washington.edu (J.J. Riley).
[1] Tel.: +1 5093353223.
[2] Tel.: +33 130 877257.
[3] Tel.: +1 206 543 5347; fax: +1 206 685 8047.

0301-9322/$ - see front matter © 2008 Elsevier Ltd. All rights reserved.
doi:10.1016/j.ijmultiphaseflow.2008.04.002

as the crossing-trajectory effects (CT) (Yudine, 1959; Csanady, 1963). The external force causes particle paths to deviate from the paths of the surrounding fluid elements and causes the particles to diffuse less than fluid elements. The CT forces particles to leave eddies prematurely and reduces T_{Lp}, which results in reduced particle diffusivity. Thus CT always reduces particle diffusivity.

The effect of inertia and CT on heavy particle dispersion was mathematically quantified by Wang and Stock (1993). They related the particle dispersion statistics to measurable flow statistics and particle parameters through algebraic equations for the normalized particle diffusivity ϵ_p, rms fluctuating particle velocity v'_p and the particle Lagrangian time scale T_{Lp}. Their equations show that for a very large drift parameter ($Dr = \tau_p \cdot q/u'_f$)[4] the heavy particle diffusivity is smaller than the fluid element diffusivity and insensitive to the inertia parameter ($St = \tau_p/T$).[5] For small drift parameters (less than 1 for dispersion in a direction perpendicular to the drift and less than 2 for dispersion in a direction parallel to the drift), particle dispersion increases with increasing inertia. Wang and Stock concluded that solid heavy particles can disperse faster than fluid elements if the inertia parameter controls the dispersion and slower than fluid elements if the drift parameter controls the dispersion. The core region of pipe flow is nearly homogeneous and isotropic and the work on particle dispersion in isotropic turbulence can be used to give a qualitative understanding of particle dispersion in this region.

Near the pipe walls there is considerable shear and turbulent dispersion of solid particles becomes more complicated. In the high-shear region particles experience a lift force due to the shear and very near the wall the particle drag is affected by the presence of the wall.

Some understanding of the seemingly contradictory experimental results of large particles dispersing more than small ones can be gained from the theoretical analysis developed for particle dispersion in homogeneous and isotropic turbulence and also by some physical shear-related considerations. However, developing a mathematical or numerically based understanding of heavy particle dispersion in turbulent shear flows remains crucial. Numerical simulations of particle dispersion in pipe flow can add additional insight to the experimental studies. With the recent advances in computing resources, large eddy simulation (LES) coupled with Lagrangian particle tracking have become powerful tools for investigating particle-laden turbulent flows.

In the study described in this paper, the experiments of Arnason (1982) were simulated using LES. Some of the cases simulated involved tracking small particles through the turbulent flow. For these cases, the small-scale turbulence, which is not directly computed in LES, is important. To recover the high wave number part of the energy spectrum, a stochastic model developed by Berrouk et al. (2007) was used to model the sub-grid transport of the particles.

2. Theoretical formulation

2.1. Continuous phase

LES was used to simulate Arnason's (1982) experiments on particle dispersion in turbulent pipe flow. A Cartesian framework was used with a length equal to 8 pipe diameters to ensure that the largest scales in the flow were captured. Using an unstructured grid of 740,000 cells avoided having too many grid points in the core region of the pipe and allowed the near-wall region to be resolved. A polar grid was used for the first three layers with non-conforming embedded refinement as shown in Table 1. Then the polar grid was matched to an octahedral region in the core region of the pipe. The first grid point near the pipe wall was located at $y^+ = 1.3$, and two grid points were within the viscous sublayer. A non-uniform grid was used in the normal-to-the-wall direction within the circular part of the grid to locate more grid points in the near-wall region where steep gradients and small energy-containing eddies exist. The Reynolds number of the simulation based on the pipe diameter and the centerline velocity was 50,000.

Periodic velocity boundary conditions were used. No-slip boundary conditions were imposed at the pipe wall for all velocity components and Neumann boundary conditions were used for the pressure.

The filtered spatial and temporal evolution of an incompressible Newtonian fluid flow is governed by the following equations:

$$\frac{\partial \bar{u}_i}{\partial x_i} = 0, \tag{2}$$

$$\frac{\partial \bar{u}_i}{\partial t} + \frac{\partial \bar{u}_i \bar{u}_j}{\partial x_j} = -\frac{\partial \bar{p}}{\partial x_i} + \frac{1}{Re}\frac{\partial^2 \bar{u}_i}{\partial x_j \partial x_j} - \frac{\partial \tau_{ij}}{\partial x_j}, \tag{3}$$

where

$$\tau_{ij} = \overline{u_i u_j} - \bar{u}_i \bar{u}_j. \tag{4}$$

τ_{ij} is the sub-grid scale (SGS) stress tensor and is modelled using the algebraic eddy-viscosity model proposed by Smagorinsky (1963):

$$\tau_{ij} - \frac{1}{3}\delta_{ij}\tau_{kk} = -2\nu_{SGS}\bar{S}_{ij}, \tag{5}$$

where ν_{SGS} is the sub-grid scale viscosity:

$$\nu_{SGS} = (C_s \Delta)^2 |\bar{S}|. \tag{6}$$

C_s is a constant, and $|\bar{S}| = |2\bar{S}_{ij}\bar{S}_{ij}|^{1/2}$, where $\bar{S}_{ij} = \frac{1}{2}(\partial_j \bar{u}_i + \partial_i \bar{u}_j)$ is the resolved rate-of-strain tensor. The length scale Δ is equal to $2h$, where h is the grid spacing, and the value of the constant C_s is 0.065.

The flow is driven by a mean axial pressure gradient $-\nabla P$ that is balanced by the net viscous friction at the pipe wall. A time step, Δt, of $0.03t^*$, where t^* is a time scale defined as the ratio of pipe diameter D and velocity at the centre of the pipe u_c was used. The size of the time step was dictated by numerical stability and the time step used to calculate the particle trajectories.

The LES were initiated with a randomly generated velocity field with mean velocity and turbulent kinetic energy profiles fitted to analytical formulas (Laurence, 2006). Computations were advanced in time until $t = 900t^*$ to achieve a flow field independent of the random initial conditions. At $t = 900t^*$, the total shear stress profile for the pipe radius showed an near linear distribution, indicating that the computations had reached a nearly statistically steady state. The calculations were continued until $t = 1100t^*$ before the final statistical data were accumulated by spatial averaging in the streamwise and circumferential directions.

In LES numerical dissipation always is part of the overall dissipation and it must be accounted for in any assessment of the quality of the results. This assessment is not as straightforward as it is for a RANS computation, because of the difficulty of discriminating between the modeling errors and the numerical discretisation errors which are both functions of the grid resolution. Speziale

Table 1
Non-conforming embedded refinement in the polar part of the unstructured grid

$y^+ = u_\tau \cdot y/\nu$	Radial direction	Circumferential direction
$0 < y^+ < 30$	4 cells	256 cells
$30 < y^+ < 100$	4 cells	192 cells
$100 < y^+ <\approx 360$ ($r = (2/3)R$)	8 cells	128 cells

[4] τ_p, the particle response time, q is a body force per unit of mass and u'_f is the fluid rms fluctuating velocity.

[5] St is the Stokes number and T is the integral time scale.

(1998) stated that a reliable LES is the one that becomes a DNS when the grid resolution is as small as the Kolmogorov scales. Consequently, one cannot seek a grid independent LES solution as we usually do for RANS computations. Celik (2003) developed a method to assess the quality of LES results. They define an index of quality as the percentage of the unresolved turbulent kinetic energy to the total. If the index of quality is less than 25% the LES can be considered adequate. The index of quality for our LES is shown in Fig. 1 as function of the pipe radius. More energy is filtered out near the wall, in particular in the buffer layer (≈12%), compared to the core region of the pipe (≈8%) but, in all locations the ratio of SGS kinetic energy to total kinetic energy is less than 25%.

The single-phase LES results are in close agreement with the mean flow properties and turbulence intensities of Laufer's experiment (Laufer, 1954) and the LES of Uijttewaal and Oliemans (1996) (using same number of cells and the dynamic procedure for the SGS model).

Fig. 2 shows the Kolmogorov time and length scales and Fig. 3 shows the integral Lagrangian time scale. The integral Lagrangian time scale was approximated by Sommerfeld (1992):

$$T_L = C_T \cdot \frac{k}{\varepsilon}. \tag{7}$$

The coefficient C_T is set to 0.3 as suggested by Milojevic et al. (1986). The Eulerian integral time scale T_E can be approximated from the Lagrangian time scale using $T_E = T_L/\beta$ with $\beta = 0.356$ (Wang and Stock, 1993).

2.2. Dispersed phase

Solid particles were released and tracked from a point source located at the center of the pipe. The physical properties of these solid particles are given in Table 2.

Particle trajectories were found by integrating the equations of motion developed by Maxey and Riley (1983). Because of the large difference in density between the gas and the particles only drag and body forces are important and the equations of motion reduce to

$$\mathrm{d}x_{p,i} = u_{p,i}\mathrm{d}t, \tag{8}$$

$$\mathrm{d}u_{p,i} = \frac{u_{s,i} - u_{p,i}}{\tau_p}\mathrm{d}t + g\,\mathrm{d}t. \tag{9}$$

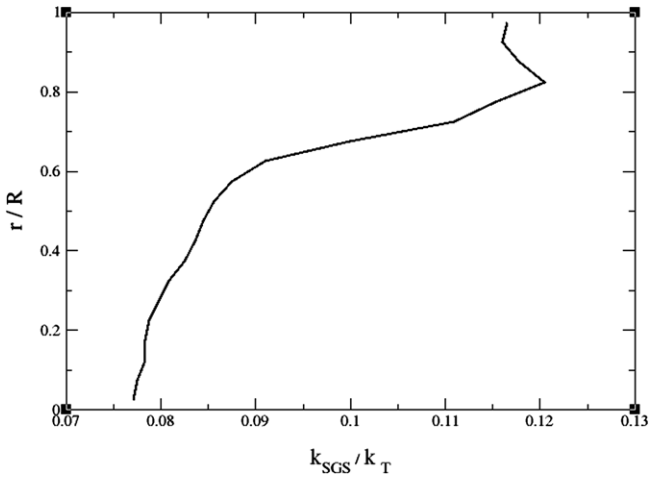

Fig. 1. Ratio of the SGS kinetic energy k_{SGS} to the total turbulent kinetic energy k_T against the non-dimensionalised pipe radius (r/R). The total turbulent kinetic energy is the sum of the SGS kinetic energy and the LES-resolved kinetic energy $k_T = k_{SGS} + k$.

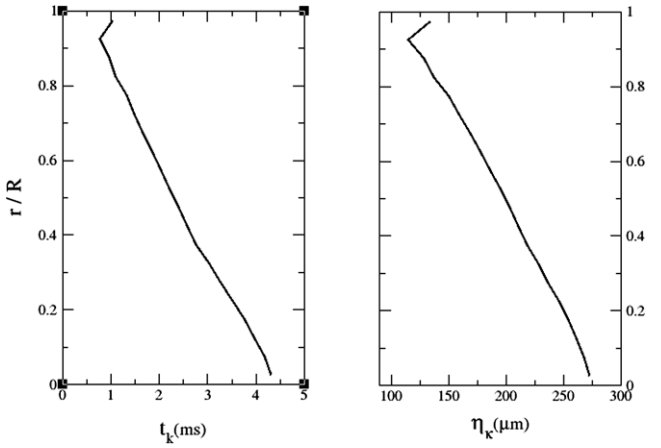

Fig. 2. LES predictions of Kolmogorov time scale t_k and length scale η_k against the non-dimensionalised pipe radius (r/R).

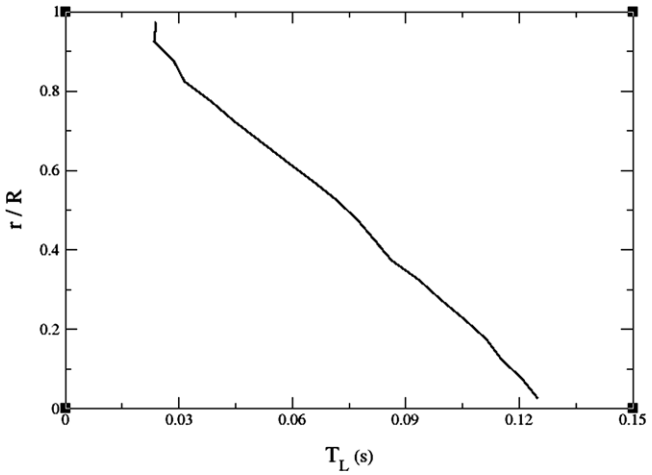

Fig. 3. LES predictions of Lagrangian time scale of turbulence T_L against the non-dimensionalised pipe radius (r/R) computed using Eq. (7).

Table 2
Physical characteristics of inertial particles used in the simulations

Mean diameter d_p^μ (μm)	5	37	57
Standard deviation σ_p (μm)	1	8	11
Clipping (μm)	$2 < d_p^\mu < 10$	$18 < d_p^\mu < 75$	$32 < d_p^\mu < 101$
Density (kg/m^3)	2475	2450	2420
Response time (m s)	0.2	10	25
Settling velocity (mm/s)	1.96	98	245

Here x_p and u_p are the particle position and velocity, u_s is the fluid velocity along the particle trajectory, g is the gravity force per unit mass and τ_p is the particle response time.[6]

In some of the particle trajectory calculations the particle Reynolds number ($Re_p = d_p|u_s - u_p|/\nu$) exceeds one, therefore a non-linear drag coefficient given by Eq. (11), must be used. When the particle Reynolds number exceeds one the drag decreases and the particle response time is given by

$$\tau_p = \frac{\rho_p}{\rho_f}\frac{4d_p}{3C_D|u_s - u_p|}, \tag{10}$$

$$C_D = \begin{cases} \frac{24}{Re_p}(1 + 0.15Re_p^{0.687}) & \text{if } Re_p < 1000, \\ 0.44 & \text{if } Re_p > 1000. \end{cases} \tag{11}$$

[6] $\tau_p = \frac{\rho_p d_p^2}{18\mu}$, ρ_p, d_p and μ are particle density and diameter and fluid viscosity respectively.

The equations of motion for a particle are only valid if the particle diameter is smaller than the Kolmogorov length scale. As shown in Fig. 2, the Kolmogorov length scale varies from 250 μm near the pipe centre to 100 μm near the wall. The largest particle diameter considered in this work is 57 μm, well within the size limit for the equations of motion.

The velocity of the fluid along the particle trajectory, u_s, depends on both the resolved, large scale turbulence and on the small scale, subgrid scale turbulence. The large scale turbulence is provided directly by the LES and the sub-grid scale turbulence which is nearly isotropic and homogeneous can be modeled by a stochastic diffusion process of Langevin type (Eq. (12)). The theoretical and numerical formulations of this model are described by Minier and Peirano (2001, 2004) in the RANS framework and its extension to model particle transport by sub-filter motion for LES is given by Berrouk et al. (2007)

$$\mathrm{d}u_{s,i} = \left(-\frac{1}{\rho_f}\frac{\partial \bar{p}}{\partial x_i} + \frac{1}{Re}\frac{\partial^2 \bar{u}_i}{\partial x_j \partial x_j}\right)\mathrm{d}t - \left(\frac{u_{s,i} - \bar{u}_i}{T_i^*}\right)\mathrm{d}t + \sqrt{C^d < \epsilon_r >}\,\mathrm{d}W_i. \quad (12)$$

Here ϵ_r is the dissipation rate of the residual or sub-filter turbulent kinetic energy k_r, C^d is the diffusion constant and dW is a Wiener process (white noise). The fluid Lagrangian time scale along the particle trajectory T_i^* is equal to the fluid Eulerian SGS time scale $T_{E,SGS}$ in the limit of a large Stokes number. On the other hand, $T^* = T_{L,SGS}$ as the size of the particle decreases. The evaluation of the different terms of Eq. (12) taking into account inertia and cross-trajectory effects is explained in Berrouk et al. (2007) and Berrouk and Laurence (in press). Numerical issues involved in the solution of Eqs. (8)–(12) are discussed in Minier et al. (2003).

In Arnason's experiment the velocity of the fluid injecting the particles into the center of the pipe work was set equal to the velocity of the gas at the center of the pipe. In the simulation the solid particle velocity was set equal to the instantaneous velocity of the fluid at the position of the particle. The initial particle position was chosen randomly on a cross-section of 3 mm in diameter that corresponded to the injection tube diameter.

The collision of the solid particles with the wall was considered perfectly elastic. According to the Sommerfeld criterion (Sommerfeld, 1992), the turbulence level and the size of the particles used in Arnasons experiment and in the numerical simulations do not give rise to a wall-collision dominated flow. The minimum particle diameter needed for the flow to be dominated by wall collision is $d_p = 108$ μm. For the particle loading used in the experiment (volume fraction $\alpha_p < 10^{-6}$), neither two-way coupling nor particle–particle collision were important.

The particles were injected at time $t = 1100t^*$ and calculations are advanced in time using the same time step $\Delta t = 0.03t^*$ used for the single-phase computations. The size of the time step was set to an order of magnitude smaller than the relaxation time of the smallest particles to avoid numerical stiffness when solving the SDE systems (Minier et al., 2003). After $t = 100t^*$,the number of particles in the flow domain became stationary and collection of particle statistics was started. For the heaviest particles used in the simulation this is equal to 40 relaxation times. Data collection lasted for $t = 100t^*$. In this interval, the statistical data were accumulated by spatial averaging in circumferential direction for each axial location. The time interval of $t = 100t^*$ was long enough to allow solid particles to adjust to the surrounding fluid before their statistics are collected.

The *Code_Saturne* was used to integrate the Lagrangian particle equations of motion. The continuous fluid phase was computed on a grid in an Eulerian framework and the dispersed phase was tracked in Lagrangian coordinates. The Lagrangian computations use the grid flexibility inherent in *Code_Saturne*. It uses a trajectography engine that allows tracking of particles in a fully unstructured grid. The strategy followed in *Code_Saturne* is called *Straight Walk*. This strategy is simple but it is not the most efficient compared to the *Orthogonal Walk* or *Visibility and Stochastic Walk* strategies (Devillers et al., 2002, 2004).

The original simulation of particle-laden flows in *Code_Saturne* was built around a RANS solution for the gas flow field. The carrier phase was simulated using one of the RANS closure schemes and then the mean flow field and turbulence scales are used in the Lagrangian module to construct the Lagrangian particle trajectories using a stochastic diffusion process of Langevin type (Minier and Peirano, 2001, 2003). For this study the Lagrangian module was extended to allow the continuous phase to be computed using LES as described in Berrouk et al. (2007) and *Code_Saturne* is used to provide the sub-grid scale velocity of the fluid at the location of a particle.

3. Results and discussion

Particle concentration and radial fluid velocity data for three different particle diameters, 5, 37 and 57 μm, were collected during the simulations. Using a method developed by Arnason and Stock (1984), an estimate of the local particle diffusivity can be obtained at a radial location if the flux of particles is caused only by gradient diffusion (Fick's law). The particle dispersion coefficient at every radial location can be computed using Eq. (13).

$$\epsilon_p = -\bar{v}_p \cdot C\left(\frac{\partial C}{\partial r}\right)^{-1}. \quad (13)$$

The concentration in every cell, C, was computed as the volume loading of every cell, i.e., the volume of all the particles present in one cell at the end of the time step divide by the volume of the cell. Then this concentration was spatial averaged over all the cells located at the same radial position for each section of the pipe (spatial averaging in circumferential direction). A third-order accurate difference scheme is used to compute the radial concentration gradients.

Figs. 4–6 show the LES predictions of the particle dispersion coefficient along with the experimental observations for the three different particle sizes. Numerical simulations that used the stochastic model for the sub-grid scale velocity agree with the experimental results for all three particle sizes. In all cases, the diffusivity computed from particle trajectories that did not include the stochastic sub-grid model were less than the experimental val-

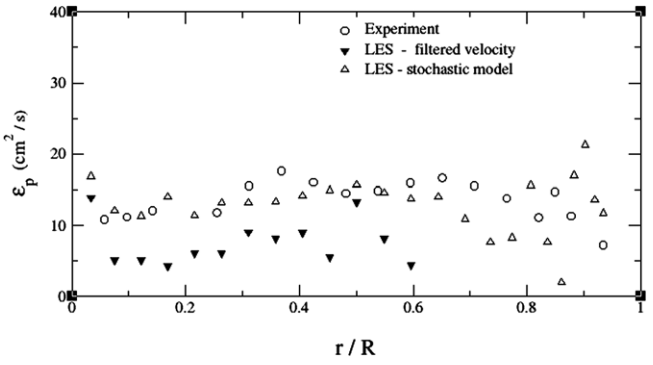

Fig. 4. Long-time particle dispersion coefficient ϵ_p for 5 μm particles versus the non-dimensionalised pipe radius. Predictions of LES using only the filtered velocity and LES using the stochastic model are compared to the experimental observations.

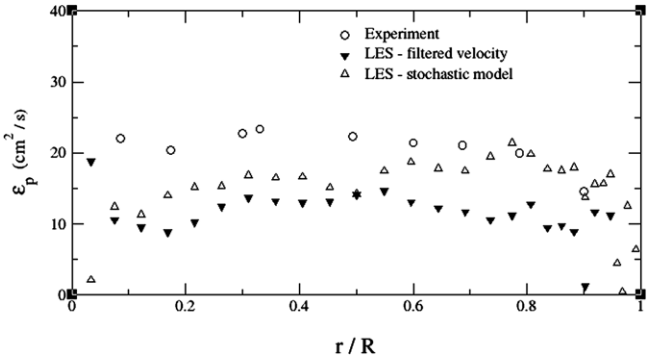

Fig. 5. Long-time particle dispersion coefficient ϵ_p for 37 μm particles versus the non-dimensionalised pipe radius. Predictions LES using only the filtered velocity and LES using the stochastic model are compared to the experimental observations.

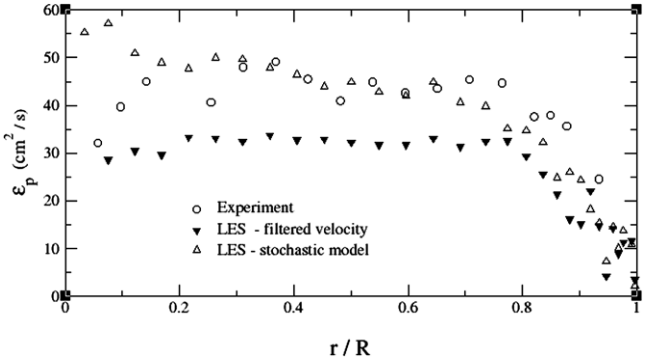

Fig. 6. Long-time particle dispersion coefficient ϵ_p for 57 μm particles versus the non-dimensionalised pipe radius. Predictions of LES using only the filtered velocity and LES using the standard formulation of the stochastic model are compared to the experimental observations.

ues. This highlights the importance of including sub-filter effects when computing particle trajectories.

Both the experimental and LES results show that the particle dispersion coefficient increases with particle diameter. The tendency of the big particles to disperse faster than the smaller particles can be seen in the particle trajectories. Fig. 7 shows instantaneous particle trajectories. Fluid element trajectories are also shown as a reference. Dotted lines represent trajectories of particles that eventually strike the wall. For clarity, particle trajectories that were concentrated near the pipe centerline were not plotted.

The effect of gravity on particle dispersion was investigated by computing particle trajectories both with and without gravity. The presence of gravity results in a finite drift or settling velocity $u_d = \tau_p \cdot g$. Fig. 8 shows the ratio of drift velocity to slip velocity for different particle diameters. The slip velocity is responsible for the viscous drag experienced by the particle. This ratio also represents the relative importance of the gravity force compared to the drag force in the particle equation of motion. For all particles, the ratio is always smaller than one and decreases as particles move away from the pipe center. The drift parameter, another measure of the relative importance of drift velocity on particle dispersion, is the ratio of the drift velocity to the radial rms fluctuating velocity. Fig. 9 shows the drift parameter for the three particle sizes. Higher values of this parameter are found at the pipe centre. The drift parameter increases with increasing particle diameter, but in all cases is less than one. For a drift parameter less than one, motion of the particles is mainly governed by the drag force and gravity has only a small effect. Turning gravity off slightly increased diffusivity of the 57 μm particles, Fig. 10. Gravity had no effect on dispersion of 5 and 37 μm particles.

Fig. 11 shows the influence of the inertia of the particle and the cross-trajectory effects on the fluid SGS time scale along the particle trajectory. Inertia and the cross-trajectory effect both play an important role in defining the time scale of the fluid along a particle trajectory. Inertia increases the time scale, whereas the cross-trajectory effect decreases the time scale of the fluid along the solid particle trajectory. As the particles move through eddies of different sizes and turbulence levels, SGS time scale decreases due to the crossing trajectories effects. The increase in time scale with increasing inertia is due to the trajectory of the heavier particles not being effect by the high frequency part of the turbulence spectrum. For this combination of flow and particles, increasing particle size decreases the fluid time scale along the particle trajectory.

The Stokes numbers based on the SGS time scales for the three particle sizes are shown in Fig. 12. Both 5 and 37 μm particles having Stokes numbers less than one are dispersed by the SGS motion. The 57 μm particles have Stokes numbers greater than one and respond less to the sub-grid scales turbulent fluctuations than the smaller particles. As expected, the SGS turbulent velocity fluctuations are more important in the trajectory calculations for particles with a Stokes number less than one.

The particle long-time dispersion coefficient strongly depends on the fluid integral time scale computed along the particle trajectory. All three particle sizes have similar fluid Lagrangian time

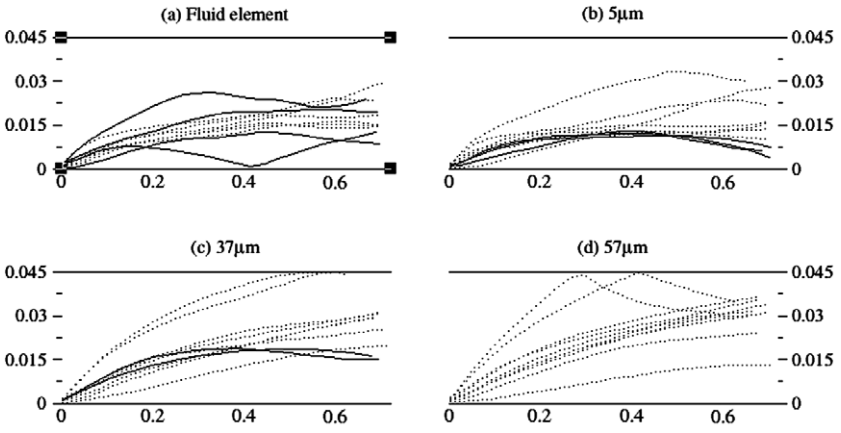

Fig. 7. LES predictions of the instantaneous particle trajectories. View in the streamwise direction: Pipe radius R = 0.045 m, pipe length L = 0.72 m. (a) Fluid particles, (b) 5 μm particles, (c) 37 μm particles, (d) 57 μm particles.

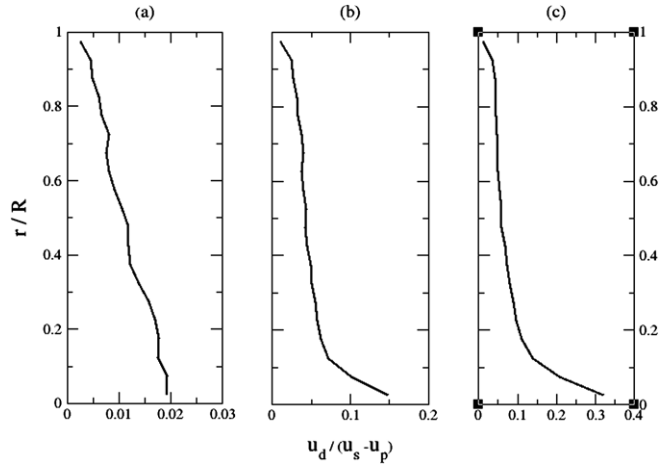

Fig. 8. LES predictions of the ratio of drift velocity u_d to streamwise slip velocity $(u_s - u_p)$ versus the non-dimensionalised pipe radius. (a) 5 μm particles, (b) 37 μm particles, (c) 57 μm particles.

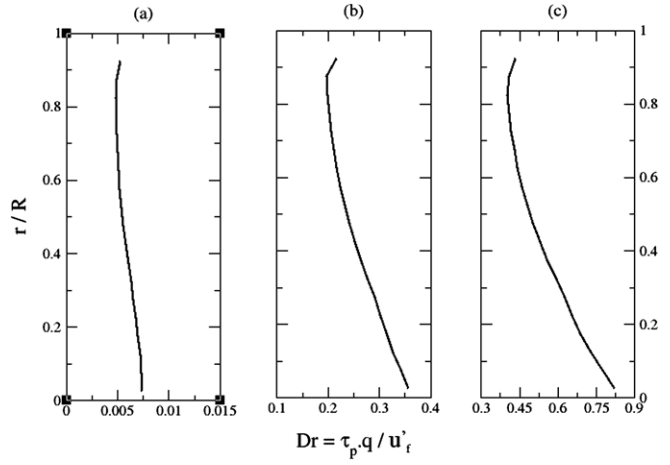

Fig. 9. LES predictions of the drift parameter $Dr = \tau_p \cdot q/u'_f$ versus the non-dimensionalised pipe radius. τ_p is the particle response time, q is a body force per unit of mass and u'_f is the fluid rms fluctuating velocity. (a) 5 μm particles, (b) 37 μm particles, (c) 57 μm particles.

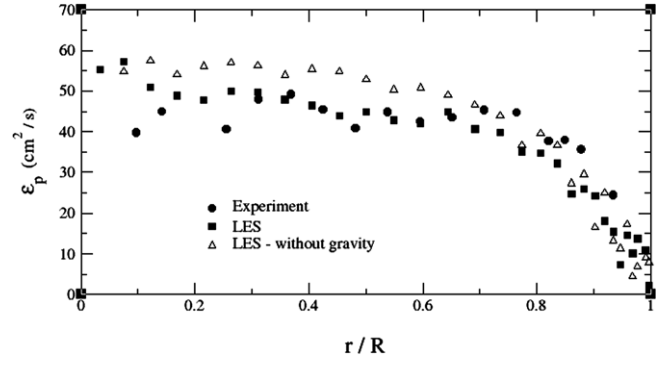

Fig. 10. Effect of gravity on LES predictions of the 57 μm dispersion coefficient.

scales. Particle trajectories depend on inertia and free-fall velocity and therefore will not, in general, sample the same turbulence. Fig. 13 shows Stokes number, based on the fluid integral time scale along the particle trajectory, for the three particles as a function of pipe radius. The 5 and 37 μm particles have Stokes numbers less

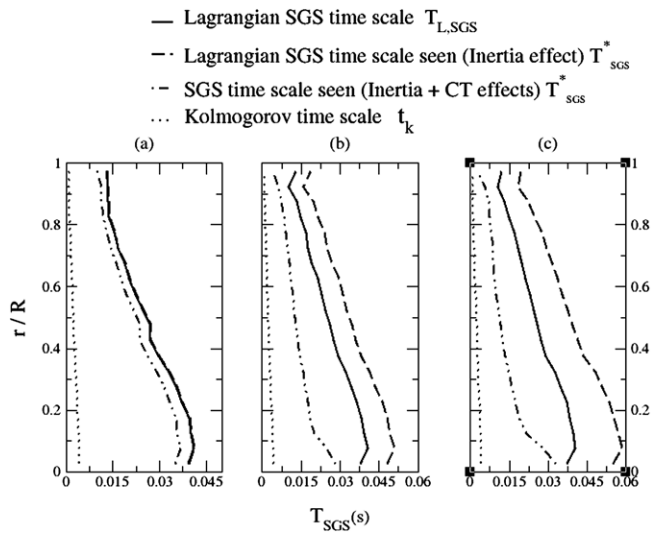

Fig. 11. Lagrangian SGS time scale T_{SGS} with which particles see the SGS turbulence versus the non-dimensionalised pipe radius. Inertia and cross-trajectory effects (CT) are included. Kolmogorov time scale t_k presented also for comparison. (a) 5 μm particles, (b) 37 μm particles, (c) 57 μm particles.

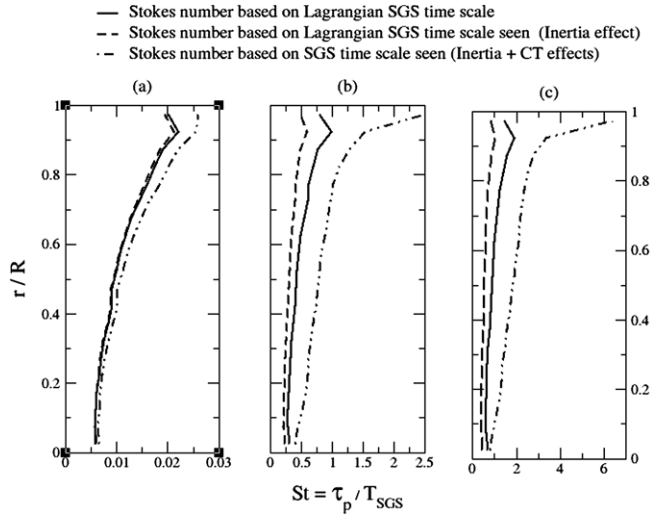

Fig. 12. Particle Stokes number based on Lagrangian SGS time scale T_{SGS} versus the non-dimensionalised pipe radius. (a) 5 μm particles, (b) 37 μm particles, (c) 57 μm particles.

than one and the 57 μm particles have Stokes number of about one. We expect the 5 and 37 μm particles to respond to most of the fluctuations related to the larger eddies and the 57 μm particles to respond to a smaller portion of the large eddies.

Fig. 14 shows the diffusivity of fluid particles and 5 μm particle as a function of pipe radius computed from LES results without using the sub-grid scale stochastic model. Numerical results are compared to an empirical estimate of fluid particle diffusivity by Vames and Hanratty (1988). These researchers stated that the fluid particle diffusivity, normalised by the kinematic viscosity and divided by the friction Reynolds number, should be a constant equal to 0.037; i.e $\epsilon_f/\nu/Re_\tau = 0.037$. This empirical result was derived from several experimental studies of pipe flow (Uijttewaal and Oliemans, 1996) and is only valid for pipe Reynolds numbers (based on mean velocity) ranging from 10^4 to 10^5. Based on this empirical formula, the fluid particle diffusivity for the present case is $\epsilon_f \approx 14$ cm^2/s. Fig. 14 shows predictions of fluid element diffusiv-

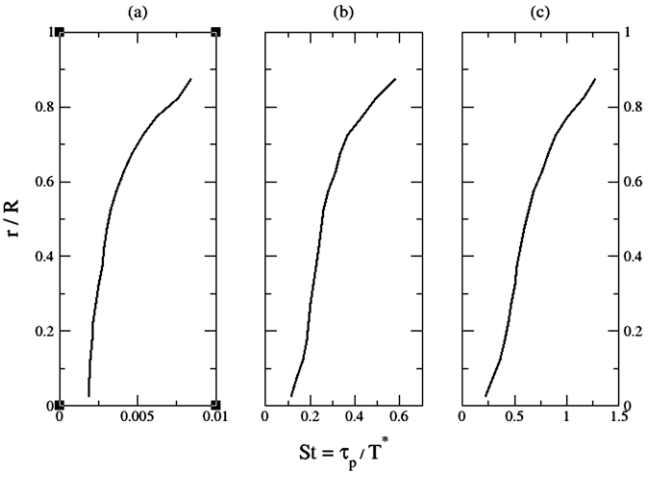

Fig. 13. Particle Stokes number based on Lagrangian time scale T^* versus the non-dimensionalised pipe radius. (a) 5 μm particles, (b) 37 μm particles, (c) 57 μm particles.

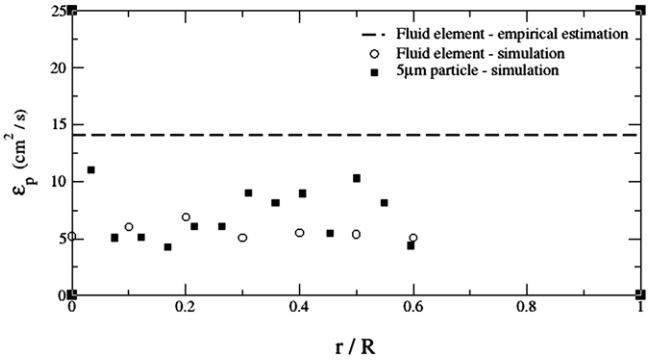

Fig. 14. LES predictions of a fluid particle diffusivity versus the non-dimensionalised pipe radius. Empirical estimation of fluid particle diffusivity according to Vames and Hanratty [Ref. 37] and LES predictions of dispersion coefficient of 5 μm solid particle are presented for comparison. Only the filtered velocity is used to track the fluid particle and the 5 μm solid particle.

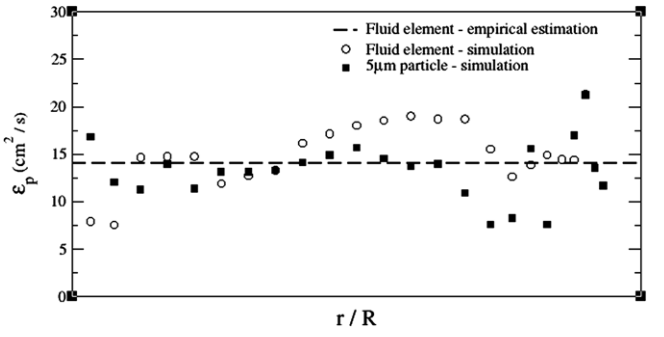

Fig. 15. LES predictions of a fluid particle diffusivity versus the non-dimensionalised pipe radius. Empirical estimation of fluid particle diffusivity according to V-ames and Hanratty [Ref. 37] and LES predictions of dispersion coefficient of 5 μm solid particle are presented for comparison. The stochastic model is used to track the fluid particle and the 5 μm solid particle.

ity without the sub-filter stochastic model underestimate the fluid particle diffusivity. Very good agreement with the empirical value of fluid particle diffusivity was obtained when the sub-filter stochastic model was used, Fig. 15.

Particle diffusivity was also computed for 105, 150 and 200 μm diameter particles. Fig. 16 shows predictions of the particle diffusivity, non-dimensionalized by fluid particle diffusivity (ϵ_f = 14 cm^2/s) as a function of the particle Stokes number based on the fluid Lagrangian integral time scale. The evolution of the normalised particle diffusivity as a function of Stokes number is similar to the trend obtained by Tang et al. (1992) for particle dispersion in a spatially developing plane mixing layer. At very small Stokes numbers, solid particles behave like fluid particle. Particle diffusivity increases with Stokes number until it reaches a peak near $St = 1$. It keeps this maximum value until around $St = 3$ ($St = 10$ for the plane mixing layer) and then decreases as the Stokes number increases.

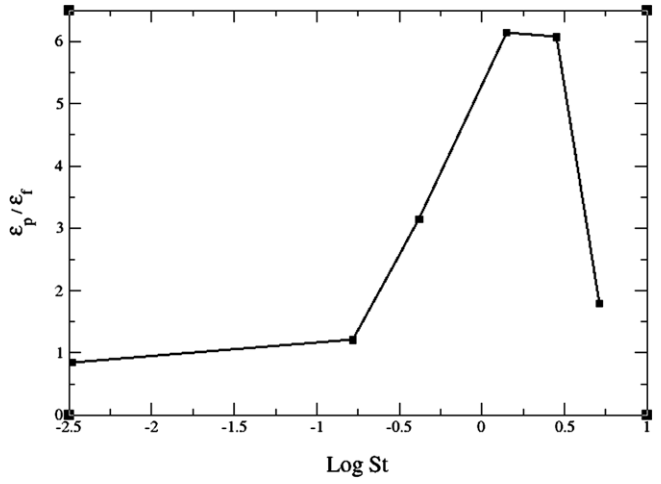

Fig. 16. LES predictions of particle dispersion coefficient non-dimensionalised by fluid particle diffusivity versus Stokes number in logarithmic scale, $St = \tau_p/T^*$.

4. Concluding remarks

Our LES simulations of heavy particle dispersion from a point source in a turbulent pipe flow and the experiments of Arnason show that particles with high inertia can disperse faster than smaller particles in turbulent pipe flow. This phenomenon was predicted by theoretical and numerical investigations of heavy particle dispersion in homogeneous and isotropic turbulence. In the presence of a shear, the situation is more complex and a numerical simulation was needed to understand the effect of inertia and free-fall velocity on particle dispersion. The simulations provide statistics of the particle motion that can help understand the dispersion process.

The particle Stokes number was the major factor controlling the dispersion and the drift parameter had an almost insignificant effect on the particle dispersion. These finding are in accord with the theoretical work of Wang and Stock (1993). The Stokes number is defined as the ratio of the particle response time to the fluid integral time scale. For our flow, the fluid integral time scales along the particle trajectories were almost the same for all three particle sizes, but the particle response time, which depends on the particle diameter squared, increased as the particle size increased. The heavier particles tended to continue in a set direction longer than the lighter particles, which resulted in a larger particle integral time scale and higher diffusivity.

The particle drift parameter is the ratio of the free fall velocity to the fluid rms velocity in the direction of the dispersion. For our flow, the drift parameter was between 0.6 and 0.007. The drift parameter needs to be one or larger before the free-fall velocity significantly affects the dispersion. The simulations done with and without gravity give almost identical dispersion, thus confirming that drift velocity had almost no effect on the dispersion.

Particle dispersion can also be explained in terms of inertia and the crossing-trajectory effects. In the absence of gravity, as inertia increases, particles set in motion by a large eddy tend to continue moving in the same direction longer, resulting in a larger integral time scale and increased dispersion. However, increased inertia also reduces the particle rms velocity, which decreases particle diffusivity as shown by Taylor (1921), Eq. (1). The relative importance of these two competing influences depends on the nature of the turbulence in the flow. For our flow and without gravity, the diffusivity increases as the particle inertia increases.

Heavy particles have a free fall velocity relative to the mean gas velocity due to gravity. This free-fall velocity causes a particle to leave an eddy before the eddy has broken up, resulting in the time scale of the particle being less than the time scale of the eddy. This phenomenon is known as the crossing-trajectory effects (Yudine, 1959; Csanady, 1963), and always decreases particle diffusivity. For our flow and particles the free fall velocity is too small for the crossing-trajectory effects to influence the dispersion.

The insight gained from our LES simulation of Arnasons experiment helps explain why the large particles can disperse more than small ones. Dispersion is influenced more by inertia of the particles than by free-fall velocity. For our particular combination of turbulence and particles, diffusivity increases along with increasing particle size.

References

Arnason, G., 1982. Measurement of particle dispersion in turbulent pipe flow Ph.D. dissertation, Washington State University, Pullman, 183pp.

Arnason, G., Stock, D.E., 1983. Dispersion of particles in turbulent pipe flow. American Society of Mechanical Engineers. Fluid Eng. Div. 10, 25–29.

Arnason, G., Stock, D.E., 1984. New method to measure particle turbulent dispersion using Laser Doppler Anemometer. Exp. Fluids 2, 89–93.

Berrouk, A.S., Laurence, D., Riley, J.J., Stock, D.E., 2007. Stochastic modelling of inertial particle dispersion by subgrid motion for LES of high Reynolds number pipe flow. J. Turbul. 8, N 50.

Berrouk, A.S., Laurence, D., in press. Stochastic modelling of aerosol deposition for LES of 90° bend turbulent flow. Int. J. Heat Fluid Flow. doi:10.1016/j.ijheatfluidflow.2008.02.010.

Calabrese, R.V., Middleman, S., 1979. The dispersion of discrete particles in a turbulent fluid field. AIChE J. 25, 1025–1035.

Celik, I.B., Cehreli, Z.N., Yavuz, I., 2003. Index of quality for large-eddy simulations. In: Proceedings of ASME FEDSM2003-45448. 4th ASME JSME joint Fluids Engineering Conference. Honolulu, Hawaii.

Crowe, C.T., Gore, R.A., Troutt, T.R., 1985. Particle dispersion by coherent structures in free shear flows. Part. Sci. Technol. J. 3, 149–158.

Csanady, G.T., 1963. Turbulent diffusion of heavy particles in the atmosphere. J. Atmos Sci. 20, 201–208.

Douce, A., 2004. *Modelisation stochastique Lagrangienne d'ecoulements turbulents diphasiques polydisperses dans Code_Saturne*. HI-81/04/03/A. Internal Report EDF R&D.

Devillers, O., Pion, S., Teillaud, M., 2002. Walking in a Triangulation. Int. J. Found.Comput. Sci. 13, 181–199.

Jones, B.G., 1966. An experimental study of the motion of small particles in a turbulent fluid field using digital techniques for statistical data processing. Ph.D. thesis. University of Illinois-Urbana.

Laufer, J., 1954. The structure of turbulence in fully developed pipe flow. NACA Rep. 1174.

Laurence, D., 2006. Large eddy simulation with unstructured finite volumes. In: Direct and Large Eddy Simulation VI. ERCOFTAC Series, vol. 10, pp. 27–38.

Maxey, M.R., Riley, J.J., 1983. Equation of motion for a small rigid sphere in a nonuniform flow. Phys. Fluids 26, 883–889.

Milojevic, D., Borner, Th., Durst, F., 1986. Prediction of turbulent gas-particle flows measured in a plane confined jet. PARTEC, Reprints 1st World Congress Particle Technology, Part IV 485–505.

Minier, J-P., Peirano, E., 2001. The PDF approach to turbulent polydispersed two-phase flows. Phys. Rep. 352, 1–214.

Minier, J-P., Peirano, E., Chibarro, S., 2003. Weak first and second order numerical schemes for stochastic differential equations appearing in Lagrangian two-phase flow modelling. Monte Carlo Meth. Appl. 9, 93–133.

Minier, J.P., Peirano, E., Chibbaro, S., 2004. PDF model based on Langevin equation for polydispersed two-phase flows applied to a bluff-body gas-solid flow. Phys. Fluids 16, 2419–2431.

Nir, A., Pismen, L.M., 1979. The effect of a steady drift on the dispersion of a particle in turbulent flow. J. Fluid Mech. 94, 369–381.

Reeks, M.W., 1977. On the dispersion of small particles suspended in an isotropic turbulent field. J. Fluid Mech. 83, 529–546.

Smagorinsky, J., 1963. General circulation experiments with the primitive equations. Mon. Weather Rev. 91, 99.

Sommerfeld, M., 1992. Modelling of particle-wall collisions in confined gas-particle flows. Int. J. Multiphase Flow 18, 905–926.

Speziale, C.G., 1998. Turbulence modelling for Time-Dependant RANS and VLES: A Review. AIAA J. 36.

Tang, L., Wen, F., Yang, Y., Crowe, C.T., 1992. Self-organising particle dispersion mechanism in free shear flows. Phys. Fluids A4, 2244–2251.

Taylor, G.I., 1921. Diffusion by continuous movements. Proc. Roy. Soc. A 151, 421–478.

Tchen, C.M., 1947. Mean values and correlation problems connected with the motion of small particles suspended in a turbulent fluid. Ph.D. Dissertation, University of Delft.

Uijttewaal, W.S.J., Oliemans, R.V.A., 1996. Particle dispersion and deposition in direct numerical and large eddy simulations of vertical pipe flows. Phys. Fluids 8, 2590–2604.

Vames, J.S., Hanratty, T.J., 1988. Turbulent dispersion of droplets for air flow in a pipe. Exp. Fluids 6, 94.

Wang, L.P., Stock, D.E., 1993. Dispersion of heavy particles by turbulent motion. J. Atmos. Sci. 50, 1897–1913.

Yudine, M.I., 1959. Physical considerations on heavy-particle dispersion. Adv. Geophys. 6, 185–191.